Iran University of Science and Technology

Automotive Science and Engineering

Journal Homepage: ase.iust.ac.ir

ISSN: 2008-9899

Numerical and Experimental Investigation of the Crushing Performance of Perforated Thin-Walled Cylindrical Tubes

Ehsan Hosseinpour [1], Ali Moazemi Goudarzi[1*], Fattaneh Morshedsolouk[1], Hussain Gharehbaghi[2]

[1] Babol Noshirvani University of Technology

[2] Tarbiat Modares University

ARTICLE INFO

Article history:

Received : 21 Aug 2024

Accepted: 25 Jun 2025

Published: 7 Jul 2025

Keywords:

Perforated Cylindrical Thin-walled Tubes

Energy Absorption Quasi-Static Axial Compression Test

Staggered vs. Straight Perforation Patterns

Perforated

Crashworthiness

Explicit Dynamics Finite Element Analysis

A B S T R A C T

This study examines how different porosity levels and perforation patterns affect the crushing performance of thin-walled cylindrical tubes under axial loading. Nonlinear explicit finite element simulations, validated by experiments, were performed on tubes with varying porosity ratios to assess deformation modes, peak crushing forces, and energy absorption efficiencies. The study's results indicate that perforated tubes have better energy absorption characteristics than non-perforated tubes, with a 7.83% improvement in the Specific Energy Absorption value. The straight-type tube demonstrated a 1.75% higher Specific Energy Absorption and 1.23% greater total energy absorption compared to the staggered arrangement. These findings suggest the effectiveness of the straight-type design for load-bearing and energy dissipation. This research offers insights into optimizing energy-absorbing structures for impact mitigation, suggesting that the straight-type configuration may be better when structural integrity and energy absorption are crucial.

1. Introduction

Passive energy absorbers are crucial in various safety-critical industries, including automotive and aerospace applications [1-3]. These structures are used to absorb impact energy and protect vehicle occupants during collisions. Among these, thin-walled cylindrical tubes have been widely studied due to their high strength, stiffness, low weight, and efficient energy absorption characteristics. These structures dissipate impact energy primarily through plastic deformation and progressive buckling, making them ideal for crashworthiness applications [4, 5]. Perforation patterns have been introduced to modify their crushing behavior to further enhance their performance, influencing factors such as energy absorption capacity and failure modes [6]. Understanding the effects of different perforation configurations is essential for optimizing these structures for real-world applications.

Thin-walled circular tubes, which absorb energy irreversibly through controlled

*Corresponding Author
Email Address: goudarzi@nit.ac.ir
https://doi.org/10.22068/ase.2025.701

[DOI: 10.22068/ase.2025.701]

deformation, have been extensively investigated as energy absorbers in vehicles [7-9]. Their lightweight design, efficient crushing distance, and cost-effectiveness make them attractive candidates for impact mitigation systems [10]. However, research on perforated tubes remains limited, particularly regarding the influence of perforation patterns on crushing behavior. Metals such as aluminum and steel are commonly used for these tubes due to their high ductility and strength [11-13].

The pioneering research by Fairbairn and Hodgkinson on the compression behavior of such tubes laid the groundwork for understanding their failure modes and enhancing their energy absorption capacity. Their study in 1846 was among the first to investigate the compression behavior of thin-walled square and circular tubes, which were commonly used in metal bridges [14]. They identified two primary failure modes: global buckling and local buckling. They also showed that the thickness-to-diameter ratio is a critical factor in determining the failure mode. Since then, the buckling behavior of thin-walled cylindrical shells has been the subject of extensive research. Alexandre [15] conducted pioneering work on the quasi-static crushing of thin-walled tubes, introducing the concept of progressive folding as a mechanism for energy absorption, which enhances their energy absorption capacity. This folding behavior enhances the energy absorption capacity of thin-walled tubes. Later, in 1984, Abramowicz and Jones [16, 17] investigated the crushing behavior of circular and square tubes under both quasi-static and dynamic axial loading conditions. They used crushing force-deformation curves to evaluate tube behavior, providing valuable insights into their response under different loading conditions. These curves provide valuable insights into how tubes respond under different loading conditions, aiding in the design and optimization of energy-absorbing structures. In conclusion, extensive research on thin-walled tubes has deepened the understanding of their compression behavior and failure modes while leading to significant advancements in their design and application for energy absorption.

To enhance energy absorption, researchers have studied various section types and structures in thin-walled tubes[18-24]. Hamouda et al. [21] investigated energy absorption in square-section tubes and demonstrated that the thickness and length of specimens significantly influence the crushing behavior of the tubes. Yousefsani et al. [25] explored the energy absorption and axial crushing behavior of thin-walled tubes with polygonal cross-sections. Notably, they found that the addition of flanges directly impacted axial force during crushing. Nia et al. [26] investigated the energy absorption capacity of thin-walled tubes with circular and square cross-sections. Their findings revealed that circular cross-section tubes exhibit higher energy absorption capacity compared to square tubes. Yousefsani et al. [25] explored the crushing behavior of steel and aluminum thin-walled tubes with various cross-sections. Younes [27] studied the crushing behavior of steel thin-walled tubes with different cross-sections. Through simulations and experimental tests, they observed that the maximum crushing occurred in circular specimens, while the minimum occurred in triangular specimens. Notably, the circular specimens absorbed the most energy.

Holes and grooves are a practical means for enhancing energy absorption in thin-walled tubes. Wang et al. [28] stated that these features modify the tube's deformation behavior during impact, enhancing energy dissipation. Researchers have extensively studied how various imperfections affect the energy absorption behavior of thin-walled tubes. Song et al. [24] conducted a study on thin-walled square tubes with patterned windows subjected to axial crushing. Their findings revealed that optimizing the dimensions of rectangular-section windows can significantly enhance energy absorption. Moradpour et al. [29] examined the crushing behavior of AA6061 and mild steel thin-walled tubes with circular holes, analyzing parameters such as the number of rows of the holes, total hole count, and hole diameter. Montazeri et al. [30] studied the effects of grooves and holes on cylindrical tubes, evaluating specific energy absorption, initial crushing force, and total absorbed energy. Their findings revealed that grooved tubes exhibit higher ICF than holed tubes, while aluminum-holed tubes have a lower SEA than steel-holed tubes but a higher SEA than

[DOI: 10.22068/ase.2025.701]

steel-grooved tubes. Optimizing the window geometry enhances crashworthiness performance.

Building on previous studies, researchers have investigated various geometric modifications in thin-walled tubes to enhance energy absorption efficiency. Baaskaran et al. [31] conducted a comprehensive study on cylindrical thin-walled tubes made of AA2024, exploring the effect of hole shape, location, and symmetry on SEA and crushing force efficiency. Notably, the hole's location along the tube wall significantly influenced buckling and crushing behavior. An elliptical hole with a longer major axis reduced ICF, while symmetric holes increased SEA. Zhang et al. [32] investigated AA6005 square tubes. Their focus was on enhancing energy absorption by altering tube geometry, particularly through hole patterns. Mohamed Ismail [33] analyzed AA6061-O square tubes with circular, square, and diamond-shaped holes to optimize energy absorption performance. Song et al. [24] conducted a study on thin-walled square tubes with patterned windows subjected to axial crushing. Their findings revealed that optimizing the dimensions of rectangular-section windows can significantly enhance energy absorption. By carefully adjusting the window geometry, engineers can achieve improved crashworthiness performance. Hosseinipour et al. [22] investigated thin-walled steel tubes containing annular grooves. These grooves play a crucial role in determining the position of folds and controlling the buckling mode of deformation. By adjusting the groove spacing, they achieved controllable energy absorption. Grooved tubes emerged as promising candidates for enhancing crashworthiness and stability during axial crushing. Researchers also explored the effects of geometry and materials on SEA, comparing aluminum thin-walled tubes with a new grooved model to assess its efficiency under axial loading conditions [22, 34].

To bridge the gap in understanding the influence of perforations on energy absorption, this study combines quasi-static compression tests with finite element analysis (FEA) using Abaqus Explicit Dynamics. An experimental test is conducted on a thin-walled cylinder to validate the numerical models, ensuring reliability in predicting crushing behavior. Two distinct sets of FEM analyses are then performed: the first investigates the effects of staggered and straight perforation patterns on energy absorption and deformation mechanisms, while the second explores the influence of perforation on structural performance. Results are interpreted using Alexander's semi-analytical approach, providing theoretical insight into the role of geometric discontinuities in energy absorption. The findings reveal critical differences in performance between staggered and straight perforation patterns, as well as the impact of perforation on crashworthiness. By examining these two aspects within a unified framework, the study offers a comprehensive understanding of how geometric discontinuities can be optimized to enhance the design of lightweight, impact-resistant structures. This research contributes to the development of more efficient energy absorbers in safety-critical industries, providing valuable insights for future applications.

2. Methodology

In this study, an investigation is conducted into the effect of perforation patterns on the energy absorption of perforated cylindrical tubes. Initially, static compression tests were performed on two specimens: one with perforations and another without. The experimental results were then used to validate the finite element method (FEM). Subsequently, a comprehensive numerical analysis was conducted involving 12 simulations to explore the impact of different perforation patterns.

2.1. Energy Absorption

The research aimed to evaluate how perforation patterns influence energy absorption, specific energy absorption (SEA), and structural behavior during crushing. SEA, defined as the energy absorbed per unit weight, was calculated alongside force-displacement curves and failure modes for each configuration. The study provided insights into optimizing tube design for improved energy dissipation and structural efficiency, with applications in crashworthiness and lightweight structures. A comparative

[DOI: 10.22068/ase.2025.701]

approach was employed to measure the effects of perforation on crushing performance, enabling a detailed analysis of deformation mechanisms and energy absorption efficiency.

Total energy absorption (EA), specific energy absorption (SEA), peak crushing force (PCF), mean crushing force (MCF), and crash load efficiency (CLE) were utilized to assess the impact of varying perforation on the structure. The corresponding formulas are defined as follows:

1. Total energy absorption

$$EA = \int P d\delta \quad (1)$$

The query involves the compression force P and the loading displacement δ .

2. Specific energy absorption

$$SEA = \frac{EA}{m} \quad (2)$$

3. Mean crushing force

$$MCF = \frac{EA}{\delta_e} \quad (3)$$

4. Crash load efficiency

$$CLE = \frac{EA}{P_{max}\delta_e} \quad (4)$$

where EA, δ_e, m, and P_{max}represent the total energy absorption, loading displacement, the mass of the specimen, and the maximum crushing force.

2.2 Experimental Setup

2.2.1. Test specimens manufacturing and geometries

Three intact cylindrical tubes, named as P0-Tube, serving as a baseline for comparison, and three perforated cylindrical tubes, named as P5-Tube, were tested. A perforated test specimen is shown in Figure 2. The tubes had uniform thickness t of 2 mm, outer diameter D of 60 mm and the length, L of 100 mm. The holes were introduced in a straight pattern using fiber laser cutting (Figure 1), with hole diameters d of 5 mm. The perforated test specimen featured evenly spaced perforations with five holes along its height and five along its radial direction. The selection of the hole diameter and number of hole rows was guided by earlier research, which indicated that a 5 mm diameter and the use of five rows of holes provide optimal energy absorption under axial loading conditions for thin-walled tubular structures [29]. A schematic representation of the perforated test specimen is shown in Figure 3.

For the preparation of the perforated test specimens, before initiating the cutting process, the desired part design is created using CAD software, specifically SolidWorks. For tubes, a 3D model is prepared with detailed specifications, including cuts and perforations. This design is then converted into machine-readable formats (IGS). The metal tube is positioned on an automatic chuck system, which securely holds and rotates the material to facilitate multi-angle cutting. The machine is configured based on the material type, thickness, laser power, cutting speed, and assist gas pressure. The fiber laser beam, transmitted through an optical fiber, is precisely focused onto the metal surface. Assist gases, such as nitrogen or oxygen, are used to blow away molten material, resulting in clean and precise cuts. The CNC system controls the cutting path according to the design specifications. Following the cutting process, the finished parts are inspected for accuracy and quality.

2.2.2. Axial Compression Testing Setup

The study utilized a FOLAD MACHINE Hydraulic Testing Machine with a 250 kN load capacity to conduct axial compression tests on test specimens (Figure 4). During testing, the specimens were compressed between the

Figure 1: ACCURL laser tube cutting machine in operation

[DOI: 10.22068/ase.2025.701]

Figure 2: The perforated test specimen

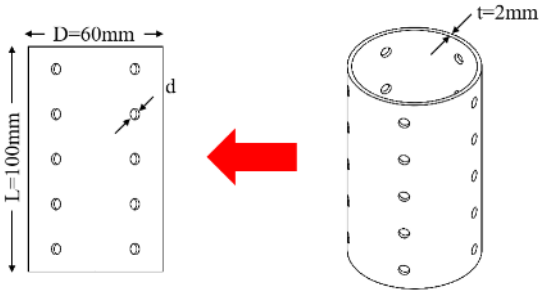

Figure 3: Schematic of P5-TUBE test specimen.

machine's platens, where the upper platen moved downward at a controlled speed of 10 mm/min to ensure the quasi-static condition of the test. This speed was specifically chosen to ensure that the tests maintained their quasi-static nature by minimizing dynamic effects. At this relatively low rate, the strain rate remains small, minimizing inertial effects and ensuring that the kinetic energy is insignificant compared to the internal energy stored in the specimen (**Figure *5***). This rate is consistent with values commonly used in similar studies [29]. Real-time force and displacement data were collected during these tests. Each experiment was repeated three times for reliability, and the average curves were used for analysis.

2.2.3. Tensile Testing and Material Characterization

Tensile tests were conducted to characterize the material properties of ST-37 steel used in this study. The test samples are cut from the intact tube using a laser cutter in the shape and dimensions shown in Figure 6. The specimens are tested under tension using the FOLAD MACHINE Machine. For enhanced precision in our analysis, we conducted tensile tests on four separate samples.

From these tests, we extracted the stress-strain curve of the steel pipe, which is shown in Figure 7. The observed deformation patterns highlight the material's ductile nature before failure, with elongation and reduction in cross-sectional area within the gauge section. This curve exhibits an initial linear elastic region followed by yielding, strain hardening, and eventual structural stability under increasing strain.

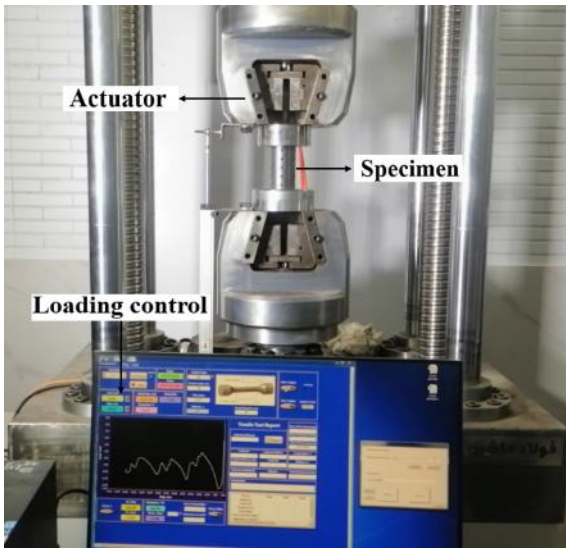

Figure 4: FOLAD MACHINE Hydraulic Testing Machine

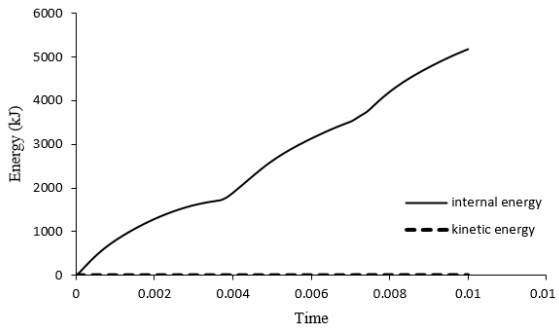

Figure 5: Internal vs. Kinetic Energy comparison.

[DOI: 10.22068/ase.2025.701]

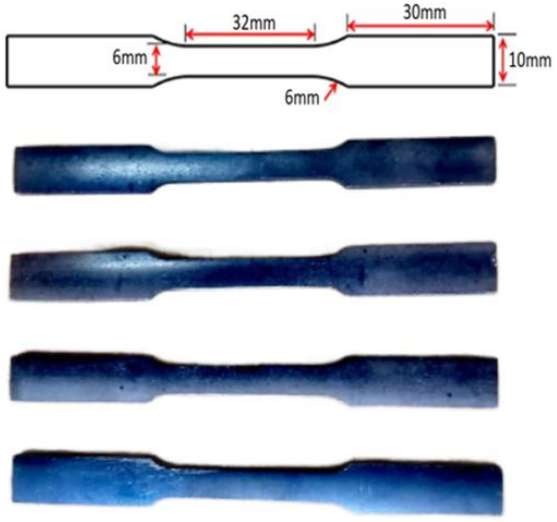

Figure 6: Tensile test specimen geometry

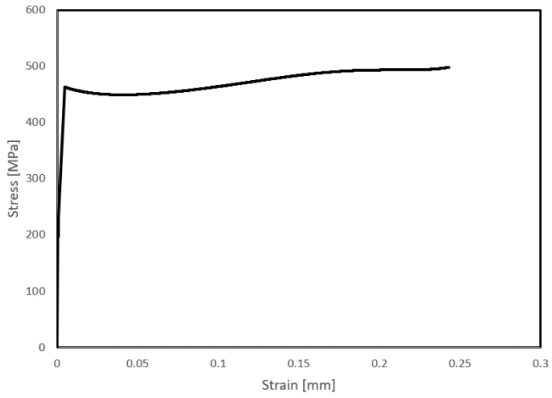

Figure 7: True stress-strain curve for ST37 steel.

This stress-strain behavior is fundamental for assessing the crushing performance and energy absorption potential of the thin-walled cylindrical tube under axial loading. Table 1 provides a summary of its mechanical properties. The mechanical properties were obtained experimentally through tensile testing by ASTM standards. During the simulation of the crushing process, the effects of material anisotropy were excluded from consideration.

Table 1: Mechanical properties of high-strength steel plates used in simulations

Material	Yield Stress [MPa]	Poisson's ratio	Young's modulus [GPa]	Density [kg/m3]
mild steel	498	0.30	197	7850

2.3 Finite Element Simulation

The finite element analysis (FEA) was conducted using Abaqus Explicit Dynamics (Version 6.6) to investigate the influence of geometric discontinuities—specifically, perforation patterns and porosity—on the energy absorption and crushing behavior of thin-walled cylinders. Two sets of FEM models were developed: one for analyzing perforation patterns and another for evaluating the effects of perforation.

2.3.1. Perforation Pattern Analysis

The cylinders are defined by their length (L), radius (R), and thickness (t), set as 100 mm, 60 mm, and 1 mm, respectively. The perforation patterns are characterized by three parameters:

- λ: Distance from the tube's edge to the center of the first perforation row.
- d: Diameter of the holes ($d = L/2n$).
- w: Spacing between adjacent hole centers in both circumferential and longitudinal directions ($w = L/n$).

here, n is the only independent variable, representing the number of holes in the longitudinal direction. The values of n range from 10 to 15. This study includes 12 numerical analyses: six for staggered perforated cylinders (SG-n) and six for straight perforated cylinders (ST-n). All specimens maintain a constant porosity of 20%. These parameters are shown for a case in Figure 8.

2.3.2. Porosity Analysis

In this study, porosity in perforated thin-walled cylindrical tubes was also investigated as it plays a crucial role in determining their structural

[DOI: 10.22068/ase.2025.701]

performance under loading. The presence of voids, which is quantified by porosity, can significantly alter a material's strength and behavior under stress. In the context of perforated tubes, porosity is affected by the distribution and density of perforations, which influence stress distribution and load transfer. To analyze these effects, the porosity of various specimens with different perforation porosities was examined. The porosity values for these specimens are presented in Table 2 below:

Table 2: Porosity values of different specimens

Specimen	Porosity (%)
P0-TUBE	0.00
P5-TUBE	2.70
P6-TUBE	3.88
P7-TUBE	5.29
P8-TUBE	6.91
P9-TUBE	8.75

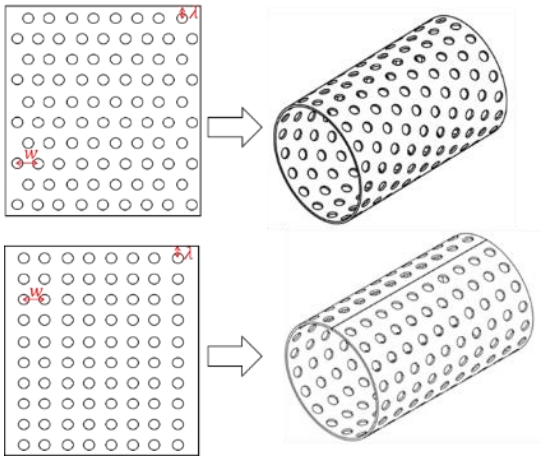

Figure 8: Parameters for ST and SG specimens

2.3.3. Material Model

The cylinders are made of ST37 tubes, assumed to be isotropic and homogeneous. Their mechanical properties are listed in Table 1. The study focuses on quasi-static crushing behavior, and the strain dependency of the material properties is neglected due to the slow application of force.

2.3.4. Crushing Simulation

In the crushing simulation, the cylinders are compressed between two test plates: The upper platen moves downward at a controlled speed until it reaches 0.6 times the length of the specimen, while the lower platen remains fixed (Figure 9). Abaqus Explicit is designed for small-duration, high-speed dynamic problems and requires small-time increments for solution accuracy. To simulate quasi-static conditions, time-scaling is applied while monitoring the ratio of kinetic energy to total energy. This ensures that the crushing process remains quasi-static. In this study, a time-scaling factor of 4×10^{-7} and a time step of 0.1 s are used [35].

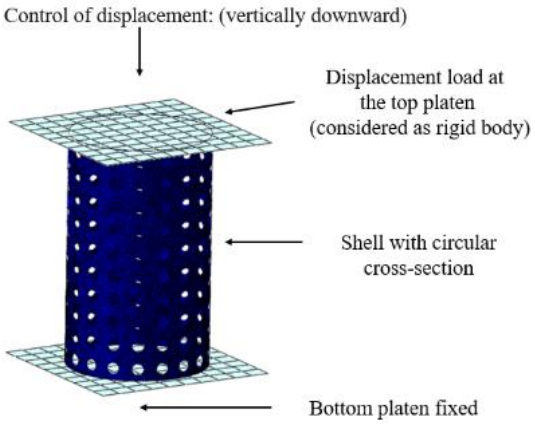

Figure 9: Finite element model of perforated cylinders

Throughout the crushing process, the total kinetic energy remains negligible compared to the total internal energy. Additionally, the load-displacement responses are unaffected by velocity, indicating that inertia effects are insignificant at the peak load value for the observed velocity range[15]. A general contact with a friction coefficient of 0.2 is defined between the platens and the specimen. After conducting a mesh sensitivity analysis, the cylinders are meshed using 28,000 S3R deformable shell elements with a size of 1 mm.

3. Results and Discussion

3.1 Validation

The accuracy of the finite element (FE) model was validated by comparing simulation results with experimental data from axial compression tests on three intact tubes (P0-TUBE specimens) and three perforated tubes (P5-TUBE specimens). The comparisons of the numerical and experimental results for P0-TUBE and P5-

[DOI: 10.22068/ase.2025.701]

TUBE specimens are shown in Figure 10 and Figure 12, respectively. The force-displacement curve obtained from the crushing test of the P0-TUBE specimen, shown in Figure *10*, indicates a 9% difference between numerical and experimental data and a 10% variation in absorbed energy. The results for the P5-TUBE specimen, shown in Figure 12, indicate a 4% difference in the initial crushing force, ICF, demonstrating a strong correlation between the two analyses.

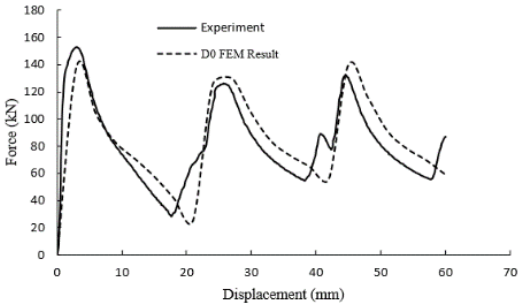

Figure 10: Force-displacement curve for P0-TUBE.

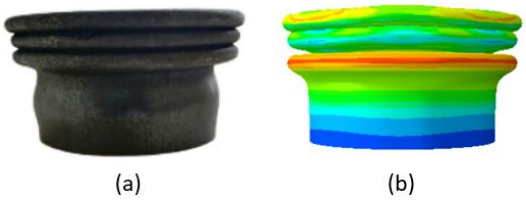

Figure 11: Comparison of hinge formation (a) experiment, (b) simulation.

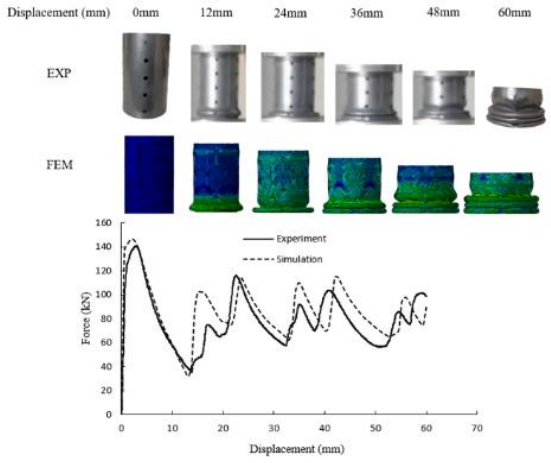

Figure 12: Deformation stages of P5-TUBE.

For the P0-TUBE specimen, it can be seen that both simulation and experiment curves initially display linear elastic behavior till the onset of the first fold. In the experiment, the first fold in the specimen formed sooner due to the small imperfection in manufacturing the tubes. After that, the behavior of the specimen will be nonlinear till the end of the experiments. By increasing the applied displacement, the force increases and it reaches the first peak, corresponding to the initial crushing force (ICF), followed by a force reduction as progressive buckling occurs. The curve demonstrates multiple peaks and valleys, reflecting the sequential fold formation and collapse of plastic hinges, as shown in Figure 11. Overall, the simulation results for the P0-TUBE specimen align well with the experimental data, with minor differences in force magnitude at certain displacement points. While the simulation slightly overestimates the force in some regions, especially near peak values, it closely follows the experimental trend. The periodic force fluctuations indicate a progressive buckling mechanism, where energy is absorbed through controlled folding. This comparison validates the finite element (FE) model's ability to accurately predict the crushing behavior of thin-walled tubes under axial loading. Additionally, as shown in Figure 11, the number of hinges observed in both the experimental and simulation tests is identical. The experimental sample exhibits clear folds that closely resemble the deformation pattern predicted by the numerical model. This confirms the FE model's accuracy, making it suitable for use in subsequent experiments.

Figure 12 illustrates the deformation stages of the P5-TUBE specimen along with its corresponding force-displacement curve. As axial load is applied and the displacement reaches 12 mm, localized deformations start to appear near the bottom edges. By 24 mm displacement, the first folding due to crushing is observed, with the upper section of the tube beginning to collapse inward, forming the initial crushing pattern.

With continued compression at 36 mm displacement, two distinct folds develop along the tube's vertical length. As displacement increases to 48 mm, the tube undergoes further

[DOI: 10.22068/ase.2025.701]

crushing, creating a more compact and densely folded structure. At this stage, the energy absorption mechanism becomes increasingly active, effectively distributing the applied load across multiple folds. By the final stage at 60 mm displacement, the tube is fully crushed, leading to a significant height reduction. The presence of holes in the tube influences the deformation pattern, enhancing its energy absorption efficiency.

Lower stress within the tube minimizes the risk of tearing and promotes the gradual formation of plastic hinges. This prevents sudden deformation that would otherwise be caused by the initial crushing force. P5-TUBE undergoes crushing without tearing, demonstrating a stable and predictable deformation pattern. Symmetry in crushing plays a vital role in energy absorption systems. The accordion-like deformation observed in holed tubes under different displacement levels exhibits high symmetry. Additionally, the crushing pattern suggests a reduced likelihood of tearing due to minimal wall elongation during plastic hinge formation. The hinges within the tube tend to align closely, further contributing to its stable deformation behavior.

3.2 Effect of Porosity on Thin-Walled Cylinders Under Crushing Test

This section evaluates how varying porosity levels influence energy absorption, specific energy absorption (SEA), and the structural behavior of thin-walled cylinders during crushing. A comparative approach measures the effects of different porosity levels on crushing performance, enabling a detailed analysis of deformation mechanisms and energy absorption efficiency.

3.2.1. Energy Absorption Parameters for Different Porosity Levels

The primary observation in this section is the consistent reduction in energy absorption parameters as porosity increases from specimen P5-Tube to P9-Tube, despite the deformation patterns remaining almost similar across all cylinders. The thin-walled cylinders (P5-Tube-P9-Tube) exhibit similar deformation patterns characterized by axisymmetric progressive x folding buckling mode, where the tubes deform through a process of progressive buckling, leading to the formation of folds along their height, as shown in Figure 13**Error! Reference source not found.** The initiation of buckling usually occurs at the bottom of the tubes by the initiation of the nonlinear region in the force-displacement region. At first, the stress concentration is higher in the vicinity of the holes, and this would control the location of the first plastic hinge. As compressive displacement increases, plastic hinges form and expand. Perforations influence deformation by encouraging controlled buckling and affecting stress distribution. The progressive collapse mechanism, characterized by localized buckling and fold formation, ensures stable energy absorption.

The deformation process is shown at six different compression displacements: 0 mm, 12 mm, 24 mm, 36 mm, 48 mm, and 60 mm. Initially, at 0 mm, all tubes retain their original cylindrical shape. As the compression increases, different buckling and crushing behaviors are observed. The P0-Tube undergoes progressive folding with a more uniform axisymmetric deformation mode. The perforated tubes (P5-Tube to P9-Tube) exhibit distinct deformation mechanisms influenced by their perforation patterns. The presence of holes seems to promote localized buckling and affect the energy absorption characteristics.

As the compression displacement increases, the tubes with perforations experience more irregular deformations, with the material folding at locations influenced by the perforation arrangement. The final deformation at 60 mm shows significant crushing in all tubes, with the perforated ones displaying more fragmented and less uniform collapse compared to the solid tube. This figure visually demonstrates the effect of perforation on the structural response of thin-walled cylindrical tubes under axial compression.

The force-displacement relationship in the thin-walled cylinders exemplified in Figure 14 for specimens P6-Tube to P9-Tube is characterized by an initial phase where the crushing force increases linearly with displacement until

[DOI: 10.22068/ase.2025.701]

localized deformations of the folds at the bottom edge of the tubes. This marks the onset of buckling. As the force continues to increase, the tube undergoes progressive buckling and folding, forming multiple folds along its height. The force-displacement curve demonstrates multiple peaks and valleys, reflecting the sequential formation and collapse of plastic hinges, where peaks often correspond to the formation of external hinges, and the lowest points indicate the creation of internal hinges. After the peak crushing force, a noticeable force reduction occurs due to plastic hinge formation. The presence of perforations influences the deformation behavior by encouraging controlled buckling and affecting stress distribution.

The perforated tubes exhibit different deformation behaviors due to variations in hole arrangement and distribution. Tubes with fewer or evenly spaced holes, like P5-Tube and P6-Tube, show more stable and sequential collapse, while those with more porosity, like P7-Tube to P9-Tube, experience earlier localized buckling and irregular folding. Overall, increasing the diameter of perforations weakens structural stability, accelerates failure, and disrupts the uniformity of the folding process.

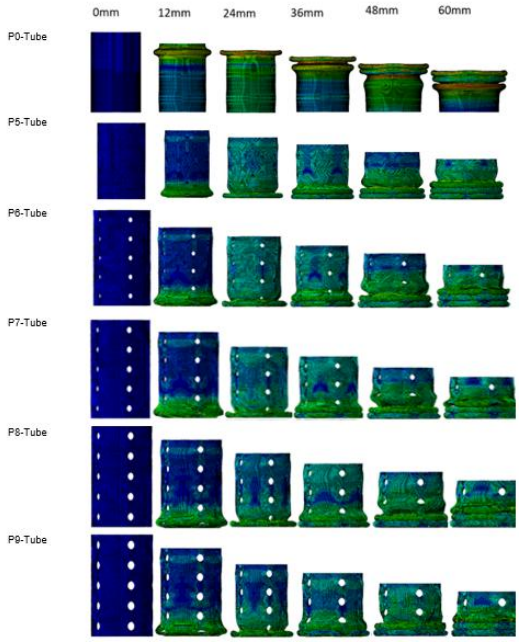

Figure 13: Deformation stages for P5-TUBE to P9-TUBE.

In this type of thin-walled structure, deformation usually starts from the tube's end and propagates upwards. In perforated tubes, the presence of holes acts as a mechanical weaknesses, altering the buckling propagation path. The folding pattern varies depending on the location and density of the perforations, leading to differences in mechanical response among the specimens.

Specimen (P0-Tube) exhibits different behavior compared to the others. This difference may be due to the absence of perforations in this sample, which increases its load-bearing capacity at this stage. In perforated samples (P5 to P9), the weaknesses induced by the holes lead to a gradual reduction in resistance, causing a more significant drop at peaks compared to P0. Next, we will examine the reason for the difference in the P9-Tube graph compared to the other graphs at the fourth peak. P9-Tube undergoes a different folding mechanism, where instead of a sharp buckle, a more gradual deformation occurs. If a complete fold does not form and a semi-stable state is maintained, the force may remain higher for a short period.

Another potential explanation is that the initiation of a new buckling mode is delayed in P9-Tube compared to the other samples. This delay could result from slight variations in stress distribution within the structure, causing the tube to sustain a higher load temporarily before a new deformation mode develops. Therefore, the most likely reason for the difference in P9-Tube within this region is a delay in the formation of a new fold or a gradual deformation pattern, causing it to sustain a higher force for a short period.

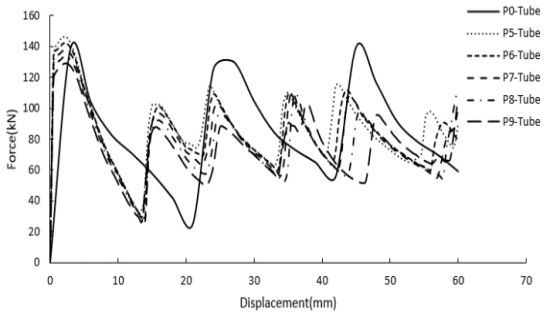

Figure 14: Force-displacement curves for P5-TUBE to P9-TUBE

[DOI: 10.22068/ase.2025.701]

Figure 15 summarizes the energy absorption parameters for specimens P5-TUBE to P9-TUBE, which exhibit a gradient in porosity from non-porous (P0-TUBE) to most porous (P9-TUBE). The specific energy absorption (SEA) demonstrates a gradual decline, decreasing from 18.65 J/g in P5-TUBE to 17.46 J/g in P9-TUBE. This trend suggests that as porosity increases, the material's ability to absorb energy per unit mass diminishes. A similar pattern is observed in the total energy absorption (EA), which drops from 5202.31 J in P5-TUBE to 4470.76 J in P9-TUBE, further reinforcing the influence of porosity on energy dissipation. The peak crushing force (PCF) and mean crushing force (MCF) also exhibit a consistent downward trend, with PCF decreasing from 145.94 kN in P5-TUBE to 128.88 kN in P9-TUBE, and MCF declining from 86.71 kN to 74.51 kN over the same range. These reductions indicate that the force required to initiate and sustain crushing diminishes as porosity increases. Interestingly, the crush efficiency factor (CEF) remains relatively stable, fluctuating only slightly between 57.58% and 59.41%, suggesting that while energy absorption and crushing forces decrease, the efficiency of the crushing process is less affected by porosity. Overall, the data reveal a clear relationship between increasing porosity and reduced energy absorption capabilities, highlighting the trade-offs between structural design and mechanical performance in porous materials.

3.2.2. Comparison of Optimal Geometry (P5-TUBE) with Non-Perforated Tube (P0-TUBE)

To further evaluate the impact of perforation, specimen P5-TUBE, identified as the optimal geometry with the highest energy absorption capacity among the perforated tubes, is compared to a non-porous thin-walled tube (P0-TUBE). Figure 16 illustrates both the P0-TUBE and P5-TUBE tubes before and after the crushing test. These tubes share the same geometric dimensions—length, thickness, and outer diameter—as the previously tested perforated tubes. Figure 15 presents a comparison of the force-displacement curves for the P5-TUBE to P9-TUBE and Intact tubes.

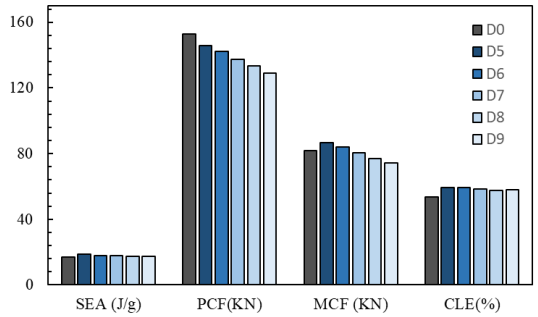

Figure 15: Energy absorption parameters vs. porosity

The P5-TUBE demonstrates a greater energy absorption capacity due to differences in the folding process compared to the P0-TUBE. In the P5-TUBE, each fold forms through a two-step mechanism: first, one half of the fold is formed, followed by the formation of the other half. This sequential folding process explains the presence of two distinct peaks in the force-displacement curve shown in Figure 16. This progressive fold formation leads to a more stable and controlled deformation pattern, contributing to enhanced energy absorption. In contrast, the P0-TUBE folds form in a single step, resulting in a different force response and folding behavior. These fluctuations enhance the energy dissipation process, leading to more efficient energy absorption. Furthermore, the reduction in peak crushing force (PCF) associated with the perforated structure contributes to improved energy absorption efficiency. The perforation also changes the deformation pattern during the crushing test. The non-perforated specimen, P0-TUBE, deformed into 4 folds, while for the perforated specimen (P5-TUBE), 3 folds were formed, Figure 17.

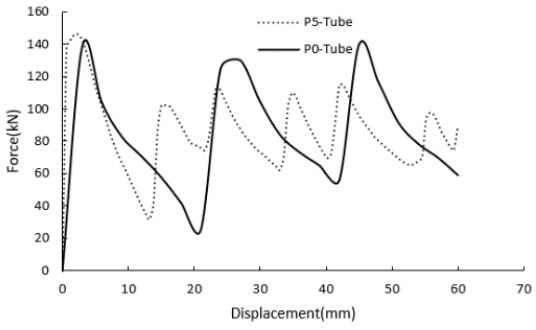

Figure 16: Force-displacement curves for P5-TUBE and Intact tubes.

[DOI: 10.22068/ase.2025.701]

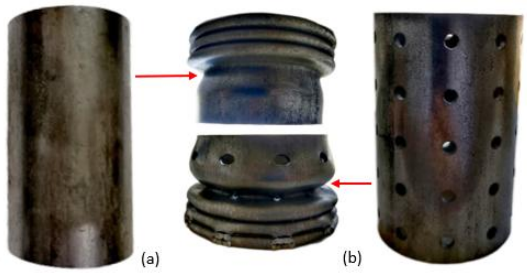

Figure 17: The samples before and after crushing, (a) P0-TUBE specimen, (b P5-TUBE specimen

The results show that the P5-TUBE tube has a higher SEA value (18.65 J/g) compared to the Intact tube (17.19 J/g), indicating improved energy absorption per unit mass. Similarly, the P5-TUBE tube demonstrates a higher EA (5202.31 J) than the Intact tube (4915.43 J), suggesting superior overall energy absorption. However, the PCF of the P5-TUBE tube (145.94 kN) is lower than that of the Intact tube (152.90 kN), implying that the latter experiences a higher peak force during crushing. The MCF values reveal that the P5-TUBE tube (86.71 kN) has a slightly higher mean crushing force compared to the Intact tube (81.92 kN), which suggests more stable deformation behavior. Additionally, the CEF for the P5-TUBE tube (59.41) is greater than that of the Intact tube (53.58), highlighting its enhanced crushing efficiency.

Overall, the P5-TUBE tube outperforms the P0-TUBE intact tube in terms of energy absorption and crushing efficiency, while the Intact tube exhibits a higher peak force during impact. One of the most notable observations is the behavior of the peak crushing force (PCF) in the intact, non-porous cylinder (P0-TUBE) compared to the porous cylinders (P5-TUBE–P9-TUBE). The PCF plays a critical role in determining the effectiveness of energy absorption, as it directly influences the initial resistance to deformation and the subsequent energy dissipation mechanisms. The higher PCF observed in the non-porous specimen (P0-TUBE) compared to the porous cylinders suggests that the absence of perforations enhances the material's ability to withstand higher initial loads, albeit at the cost of reduced energy absorption efficiency. This highlights the trade-off between structural integrity and energy absorption performance, which is significantly influenced by the presence and distribution of porosity.

3.3. Crushing Performance of Perforated Cylinders: Staggered vs. Straight Patterns

This section explores the behavior of cylindrical structures with perforations, focusing on how different configurations and design parameters influence their energy absorption capabilities. The analysis extends to cylinders with staggered perforation patterns, investigating how this arrangement affects structural performance. A comparative evaluation is provided to contrast the energy absorption characteristics of these two configurations, offering insights into their respective strengths and limitations. Additionally, the role of fold length is analyzed to understand its impact on the deformation behavior and overall energy absorption efficiency. Through this comprehensive exploration, the section aims to provide a deeper understanding of the factors that optimize the performance of perforated cylinders as energy-absorbing structures.

3.3.1. Straight-Perforated Cylinders

This study investigates the behavior of straight-perforated cylinders featuring 10 to 15 vertical holes during quasi-static compression. Figure 18 depicts the force-displacement response and failure mode of specimen ST-10, which is representative of the behavior observed in ST-11, ST-12, and ST-13 due to their consistent deformation patterns under compressive loading. After reaching the peak crushing force (PCF), the specimens underwent local buckling, forming a small fold at the top that corresponded to the peak in the load-displacement graph. As crushing displacement increased, a series of folds developed sequentially, contributing to the failure. Specimens ST-10, ST-11, ST-12, and ST-13 exhibited similar behavior, with folds forming progressively until the structure was fully crushed. In the force displacement diagram of these cylinders, each of two peaks corresponds to a fold. In contrast, specimens ST-14 and ST-15 displayed a nonsymmetric diamond combined

[DOI: 10.22068/ase.2025.701]

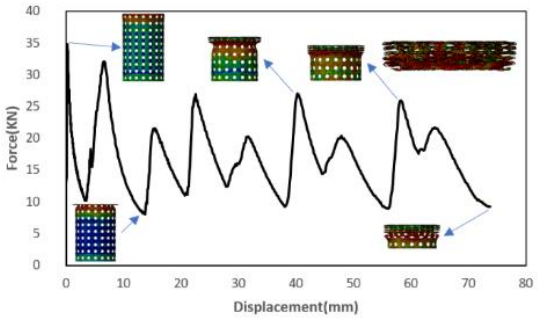

Figure 18: Force-displacement and failure modes for ST-10

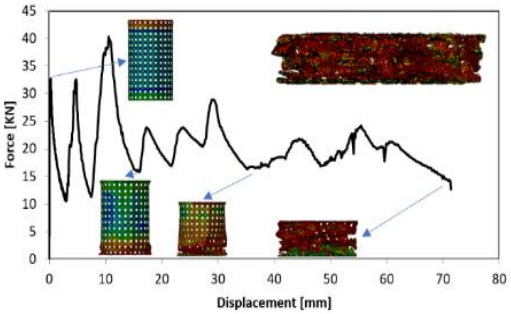

Figure 19: Force-displacement and failure modes for ST-14

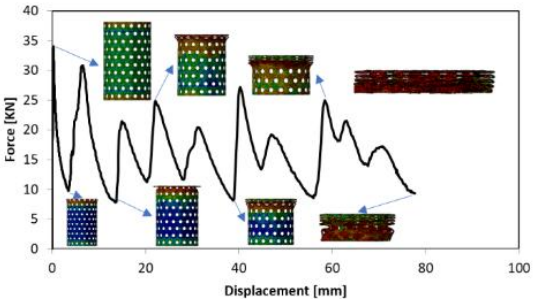

Figure 20: Force-displacement and failure modes for SG-10

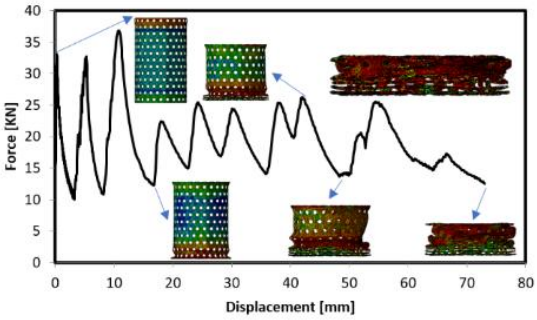

Figure 21: Force-displacement and failure modes for SG-13

failure mode. Initially, multiple folds formed gradually, followed by two simultaneous folds along the cylinder's length, which expanded with increased crushing displacement until complete collapse (see Figure 20).

3.3.2. Staggered perforated cylinders

To investigate how the shape, whether straight or staggered, affects the crushing behavior of cylinders, a numerical study was conducted on six specimens featuring a varying number of holes, ranging from 10 to 15. The force-displacement relationships for SG-10 and SG-13 and there presented in Figure 20, respectively. Analysis of the deformation patterns revealed a consistent buckling mode across SG-10, SG-11, and SG-12, which were characterized by the formation of axisymmetric folds. For the SG-13, SG-14, and SG-15, initially three folds were formed progressively, which was subsequently followed by the simultaneous emergence of two asymmetric folds.

3.3.3. Comparison of Staggered and Straight Pattern

A comparison of the crushing behavior between the SG-10 and ST-10 perforation patterns was conducted, with the results illustrated in Figure 22. The deformation of both specimens under crushing was analyzed, revealing that their failure modes were characterized by axisymmetric progressive folding. This behavior was consistent across both models. Figure 23 shows the crushing force required for ST-10 and SG-10 over a displacement of approximately 80 mm. The energy absorbed by the specimens can be determined from the area under the force-displacement curve. The initial peak in the curve represents the formation of the first fold, while the total number of peaks corresponds to the number of folds. A comparison of the crushing force reveals that the peak force, associated with the first buckling, is 34.9 kN for ST-10 and 34 kN for SG-10, a 2.6% difference. This variation arises from the specific arrangement of perforated

[DOI: 10.22068/ase.2025.701]

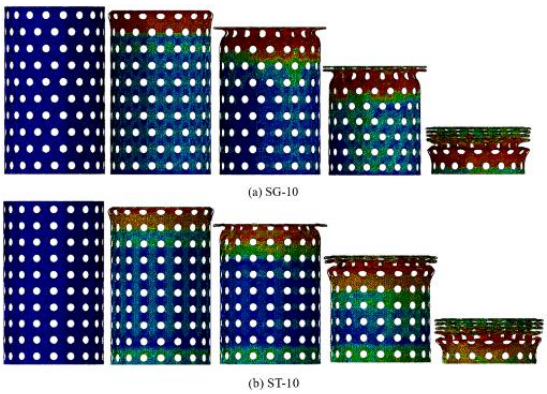

Figure 22: Deformation patterns of (a) SG-10 and (b) ST-10

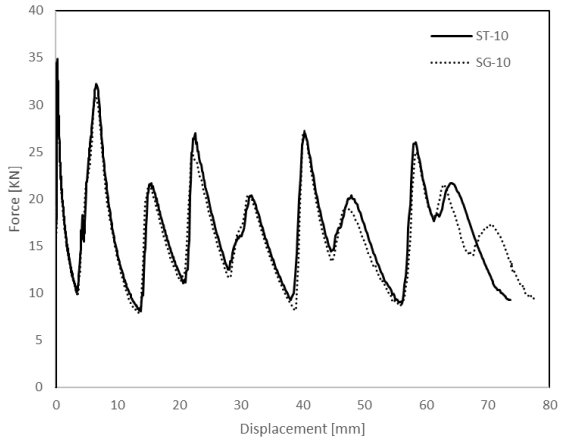

Figure 23: Force-displacement curves for SG-10 and ST-10

sheet geometries and the more uniform stress distribution in ST-10.

In ST-10, with the initiation of axial loading and an increase in the displacement of the plate, the crushing force increases linearly until a small outward fold forms at the upper edge. As the force continues to increase, this fold develops into the shape of a half-wave. The center of this fold aligns with the center of the first row of perforation. This fold is completed when the edges of the fold come into contact. The subsequent fold occurs as an inward half-wave, with its center aligned with the second row of perforation. In this manner, up to the end of crushing, the deformation and crushing behavior of the perforated cylinder are controlled by the arrangement of the perforation. In the force-displacement diagram, the onset of the second wrinkle, centered on the second row of perforation, corresponds to the beginning of the second peak. Thus, each fold centered on a row of perforations represents a peak in the graph. It should be noted that the second fold occurs on the interior and is ultimately not visible from the outside. In SG-10, the crushing occurs in a progressive folding manner, similar to ST-10, and the folding continues in a manner analogous to that observed in ST-10.

The region under the force-displacement curve indicates the total energy absorbed by the energy systems, as previously discussed. The ST-10 specimen absorbs 1.23% more energy than the SG-10. These results indicate that the straight specimen exhibits enhanced energy absorption and overall performance compared to the staggered one. The superior energy absorption performance of the straight perforation pattern compared to the staggered one can be attributed to differences in stress distribution and failure propagation. In the straight configuration, perforations are aligned along uniform axes, which promotes symmetric and progressive deformation under loading. This alignment results in a more stable crushing behavior and facilitates energy dissipation over a larger deformation range. On the other hand, the staggered pattern creates more complex and non-uniform load paths. This can cause stress concentrations around offset holes, which in turn limit the material's ability to absorb energy effectively. Since energy absorption is a critical aspect of energy-absorbing systems, the superior performance of the straight specimen is particularly noteworthy.

The energy absorption performance metrics—specifically Peak Crushing Force (PCF), Specific Absorbed Energy (SEA), and Absorbed Energy (EA)—for all specimens are displayed in Figure 24 and Figure 25. The analysis reveals that the failure modes, PCF, SEA, and EA, are largely unaffected by the transition from staggered to straight patterns and show minimal variation with changes in the number of holes along the height. Notably, the PCF is slightly lower for cylinders with a higher number of holes, showing a 6.88% reduction, and the absorbed energy also increases as the number of holes increases, with a 6.88%

[DOI: 10.22068/ase.2025.701]

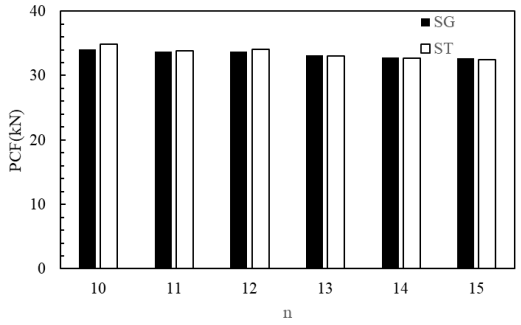

Figure 24: Comparison of Peak Crushing Force (PCF) for SG and ST patterns

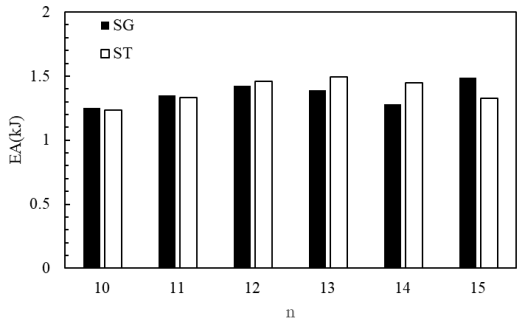

Figure 25: Comparison of Absorbed Energy (EA) for all cylinders

rise observed compared to the configuration with fewer holes.

This indicates that cylinders with more holes are less effective at energy absorption.

3.3.4. Fold Length (H) Analysis

Figure 26 illustrates a theoretical model for the axisymmetric collapse of a thin-walled cylindrical tube under axial loading by Alexander [15]. The tube's behavior during collapse is represented with geometric features such as folds and hinges.. The tube has a diameter of D, and the wall thickness is represented as h. Hinges are shown at specific locations, representing points of plastic deformation that form during the collapse process. Alexander suggested that H, the half-length of a fold, can be calculated as $H = \sqrt{\left(\frac{\pi}{2\sqrt{3}}\right)}\sqrt{Dh} \approx 0.95\sqrt{Dh}$. Based on this formulation, H for a non-porous cylinder of the dimension of ST models is 7.36 mm. It can be seen that this parameter does not depend on the length of the cylinder, and it is the minimum fold length that can be achieved in a crushing test.

In this study, it was observed that for perforated cylinders exhibiting stable axisymmetric crushing behavior, the fold half-length (H) corresponds to the total length of the cylinder divided by the number of perforation rows along its height. Figure 27 illustrates the measured half-length of the folds for specimens ST-10 to ST-13, as well as the hypothetical half-length of the folds for specimens ST-14 and ST-15, assuming an axisymmetric folding crushing mode. n is the number of rows of the perforation in the height of the cylinders.

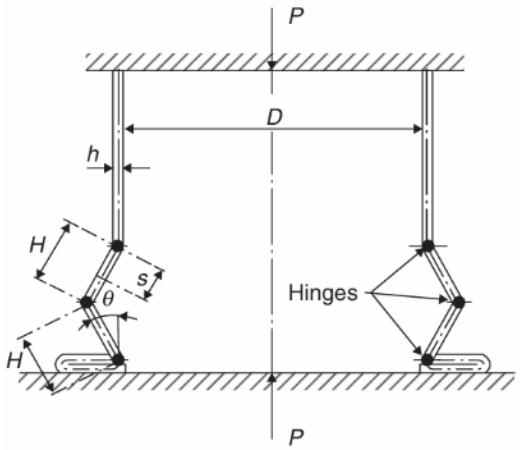

Figure 26: The Alexandre [15] model for axisymmetric collapse.

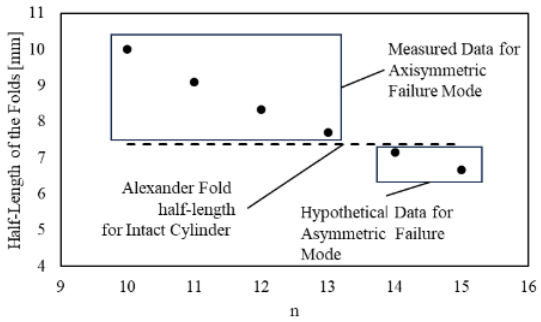

Figure 27: Axisymmetric half-length of fold for ST perforated cylinders ().

[DOI: 10.22068/ase.2025.701]

This explains why the failure mode for cylinders with 14 and 15 rows of perforations is different from the other samples. Based on the validity of the analysis results in Abaqus software, and by considering the figures and the relationships mentioned earlier, it can be observed that for an Intact cylinder without perforations, the value of H calculated using the given formula is 7.36 mm. The H values in the table have been calculated for all cylinders. For a cylinder with 10 rows of perforations, H equals 10 mm, while for other samples, this value decreases progressively, reaching 6.66 mm for the cylinder with 15 rows of perforations.

It is evident that the value of H, which corresponds to an Intact cylinder without perforations, falls between the values for cylinders with 13 and 14 rows of perforations (H=7.69 and H=7.14, respectively). The failure modes for the samples with 14 and 15 rows of perforations are distinctly different from those of the other samples. The cause of this phenomenon is related to the value of H and its influence on the failure mode of the cylinder. For cylinders with 14 and 15 rows of perforations, the value of H is less than the threshold value of 7.36 mm, and consequently, the failure mode is not axisymmetric.

These findings highlight the possibility of engineering and pre-designing the failure modes and the number of folds in cylindrical structures to achieve desired outcomes. For example, if it is required for a cylinder to form 4 folds during crushing, an arrangement with 8 rows of perforations can be employed. This configuration results in an H-value of 12.5 mm, which is greater than the threshold value of 7.36 mm, ensuring that the failure mode remains axisymmetric.

Furthermore, the ability to control and predict the failure behavior of cylindrical structures by modifying geometric parameters such as the number of perforation rows provides a powerful tool in design engineering. The relationship between H and the failure mode not only explains the observed phenomena but also enables the optimization of energy absorption, structural integrity, and performance during axial loading. The influence of H on the deformation pattern and folding mechanism is particularly crucial, as it dictates the stability and symmetry of the crushing process. Cylinders with H-values above the threshold tend to exhibit more predictable, symmetric folding behavior, while those with lower H-values deviate from this behavior, resulting in more complex, asymmetric failure modes.

This understanding can be applied across various applications, such as crashworthiness design, where controlled energy absorption is critical. By tailoring the number of perforation rows and, consequently, the H-value, engineers can ensure that the desired failure mode aligns with the functional requirements of the structure.

4. Conclusion

This study introduces a novel tube crushing technique and evaluates its performance against perforation, staggered, and straight specimens under identical conditions. We analyzed various parameters during the axial loading process, including crushing behavior, initial load peak, maximum force (Fmax), energy absorption, and specific energy absorption (SEA).

The results of this study revealed that the straight specimen outperformed the staggered workpiece in terms of force dissipation and energy absorption, despite being subjected to identical weight and conditions. The thin, staggered perforated tube demonstrated greater formability and exhibited asymmetrical decay compared to the straight specimen. Moreover, the Specific Energy Absorption (SEA) ratio of the straight perforated specimen was 1.75% higher than that of the staggered specimen, while the overall energy absorption of the straight specimen surpassed that of the staggered one by 1.23%. Additionally, the staggered perforated specimen exhibited lower force.

Adjusting the diameter of holes results in variations in energy absorption and the energy-to-weight ratio. Among the tested configurations, the P5-TUBE tube emerged as the most effective design. This configuration consists of five rows of holes, with each row containing five 5mm diameter holes.

The SEA value of the P5-TUBE tube demonstrates a 7.83% enhancement compared to

[DOI: 10.22068/ase.2025.701]

the non-perforated (intact) tube. The specimens exhibited relatively symmetrical crushing behavior and effectively dissipated energy.

These findings demonstrate the potential of perforated cylinders as energy-absorbing elements in practical applications such as automotive crash boxes, aerospace structures, and protective equipment, where efficient energy dissipation and lightweight design are critical.

Future research should investigate the behavior of perforated cylinders under dynamic or impact loading conditions to better simulate real-world crash scenarios, particularly for applications in automotive and aerospace safety systems. Evaluating the strain-rate sensitivity and energy dissipation capacity under high-speed loading will provide critical insights into their crashworthiness. Additionally, the development and testing of hybrid perforation patterns — such as combining straight and staggered configurations, implementing variable hole diameters, or applying non-uniform hole distributions along the cylinder axis — may reveal optimized designs that enhance energy absorption while maintaining structural integrity. Such investigations could lead to more efficient and application-specific crashworthy components.

Declaration of Conflicting Interests

The authors declared no potential conflicts of interest with respect to the research, authorship, and/or publication of this article.

References

1. Elyasi, M., S. Montazeri, and A. Moradpour, *Investigating the effect of material type in the new design of thin-walled tubes under axial loading.* Advances in Materials and Processing Technologies, 2015. **1**(3-4): p. 375-383.
2. Elyasi, M., A. Moradpour, and S. Montazeri, *Axial crushing in a novel technique of thin-walled tube.* Key Engineering Materials, 2014. **622**: p. 709-716.
3. Sadighi, A., et al., *A novel axially half corrugated thin-walled tube for energy absorption under axial loading.* Thin-Walled Structures, 2019. **145**: p. 106418.
4. Yao, S., et al., *Prediction and application of energy absorption characteristics of thin-walled circular tubes based on dimensional analysis.* Thin-Walled Structures, 2018. **130**: p. 505-519.
5. Aghamirzaie, M., A. Najibi, and A. Ghasemi-Ghalebahman, *Energy absorption investigation of octagonal multi-layered origami thin-walled tubes under quasi-static axial loading.* International Journal of Crashworthiness, 2023. **28**(4): p. 511-522.
6. Yian Peen, W., C. Yie Sue, and C. Kok Keong, *Effect of Perforation Area and Arrangement Pattern on Structural Behaviour of Nature Inspired Perforated Hollow Structure.* Iranica Journal of Energy & Environment, 2013. **4**(3).
7. Li, Y. and Z. You, *External inversion of thin-walled corrugated tubes.* International Journal of Mechanical Sciences, 2018. **144**: p. 54-66.
8. Rahi, A., *Controlling energy absorption capacity of combined bitubular tubes under axial loading.* Thin-Walled Structures, 2018. **123**: p. 222-231.
9. Pang, T., et al., *Energy absorption mechanism of axially-varying thickness (AVT) multicell thin-walled structures under out-of-plane loading.* Engineering Structures, 2019. **196**: p. 109130.
10. Gao, Q. and W.-H. Liao, *Energy absorption of thin walled tube filled with gradient auxetic structures-theory and simulation.* International Journal of Mechanical Sciences, 2021. **201**: p. 106475.
11. Abada, M. and A. Ibrahim, *Hybrid multi-cell thin-walled tubes for energy absorption applications: Blast shielding and crashworthiness.* Composites Part B: Engineering, 2020. **183**: p. 107720.
12. Taghipoor, H. and A. Eyvazian, *Quasi-static axial crush response and energy absorption of composite wrapped metallic thin-walled tube.* Journal of the Brazilian Society of Mechanical Sciences and Engineering, 2022. **44**(4): p. 158.
13. Wang, B. and G. Lu, *Mushrooming of circular tubes under dynamic axial loading.* Thin-walled structures, 2002. **40**(2): p. 167-182.

[DOI: 10.22068/ase.2025.701]

14. Timoshenko, S., *History of strength of materials: with a brief account of the history of theory of elasticity and theory of structures*. 1983: Courier Corporation.
15. ALEXANDER, J.M., *AN APPROXIMATE ANALYSIS OF THE COLLAPSE OF THIN CYLINDRICAL SHELLS UNDER AXIAL LOADING.* The Quarterly Journal of Mechanics and Applied Mathematics 1960. **13**(1).
16. Abramowicz, W. and N. Jones, *Dynamic axial crushing of square tubes.* International Journal of Impact Engineering, 1984. **2**(2): p. 179-208.
17. Abramowicz, W. and N. Jones, *Dynamic axial crushing of circular tubes.* International Journal of Impact Engineering, 1984. **2**(3): p. 263-281.
18. Adachi, T., et al., *Energy absorption of a thin-walled cylinder with ribs subjected to axial impact.* International journal of impact engineering, 2008. **35**(2): p. 65-79.
19. Al Galib, D. and A. Limam, *Experimental and numerical investigation of static and dynamic axial crushing of circular aluminum tubes.* Thin-Walled Structures, 2004. **42**(8): p. 1103-1137.
20. Gupta, N., *Collapse mode transitions of thin tubes with wall thickness, end condition and shape eccentricity.* International journal of mechanical sciences, 2006. **48**(2): p. 210-223.
21. Hamouda, A., R. Saied, and F. Shuaeib, *Energy absorption capacities of square tubular structures.* Journal of Achievements in Materials and Manufacturing Engineering, 2007. **24**(1): p. 36-42.
22. Hosseinipour, S. and G. Daneshi, *Energy absorbtion and mean crushing load of thin-walled grooved tubes under axial compression.* Thin-walled structures, 2003. **41**(1): p. 31-46.
23. Salehghaffari, S., M. Rais-Rohani, and A. Najafi, *Analysis and optimization of externally stiffened crush tubes.* Thin-walled structures, 2011. **49**(3): p. 397-408.
24. Song, J., Y. Chen, and G. Lu, *Light-weight thin-walled structures with patterned windows under axial crushing.* International journal of mechanical sciences, 2013. **66**: p. 239-248.
25. Yousefsani, S.A., J. Rezaeepazhand, and S. Maghami, *Axial crush of metallic and hybrid energy absorbing thin-walled tubes with polygonal cross-sections: Numerical analysis.* 2013.
26. Nia, A.A., H. Badnava, and K.F. Nejad, *An experimental investigation on crack effect on the mechanical behavior and energy absorption of thin-walled tubes.* Materials & Design, 2011. **32**(6): p. 3594-3607.
27. Younes, M. *Finite element modeling of crushing behavior of thin tubes with various cross sections*. in *13th International Conference on Aerospace Sciences & Aviation Technology, ASAT-13, Paper: ASAT-13-ST-34*. 2009.
28. Wang, W., et al., *Numerical simulation and experimental study on energy absorption of foam-filled local nanocrystallized thin-walled tubes under axial crushing.* Materials, 2022. **15**(16): p. 5556.
29. Moradpour, A., M. Elyasi, and S. Montazeri, *Developing a new thin-walled tube structure and analyzing its crushing performance for aa 60601 and mild steel under axial loading.* Transactions of the Indian Institute of Metals, 2016. **69**: p. 1107-1117.
30. Montazeri, S., M. Elyasi, and A. Moradpour, *Investigating the energy absorption, SEA and crushing performance of holed and grooved thin-walled tubes under axial loading with different materials.* Thin-Walled Structures, 2018. **131**: p. 646-653.
31. Baaskaran, N., K. Ponappa, and S. Shankar, *Quasi-static crushing and energy absorption characteristics of thin-walled cylinders with geometric discontinuities of various aspect ratios.* Latin American Journal of Solids and Structures, 2017. **14**: p. 1767-1787.
32. Zhang, L., et al., *Influence of prolonged natural aging followed by artificial aging on tensile properties and compressive behavior of a thin-walled 6005 aluminum alloy tube.* Journal of Central South University, 2021. **28**(9): p. 2647-2659.
33. Mohamed Ismail, N.M., *Performance analysis and optimization of square tubes with different shapes, sizes, and patterns of*

[DOI: 10.22068/ase.2025.701]

holes under axial compression loading. International Journal of Crashworthiness, 2024. **29**(2): p. 247-273.
34. Mamalis, A., et al., *Finite element simulation of the axial collapse of metallic thin-walled tubes with octagonal cross-section.* Thin-walled structures, 2003. **41**(10): p. 891-900.
35. *ABAQUS, Version 6.6, Documentation*. Available from: https://classes.engineering.wustl.edu/2009/spring/mase5513/abaqus/docs/v6.6/books/gsx/default.htm?startat=ch03s01.html.

[DOI: 10.22068/ase.2025.701]